Modeling and Analysis of the Current Source Characteristics of a Soft Switched Resonant Converter

Ilya Zeltser[1], *Member*, *IEEE* and Sam Ben-Yaakov[2], *Fellow*, *IEEE*

[1]Department of Applied Physics
Rafael Advanced Defense Systems Ltd.
P.O. Box 2250, Haifa 31201, Israel
Phone: +972-4-8795045; Fax: +972-4-8795315
Email: ilyaz@rafael.co.il
Website: www.rafael.co.il

[2]Power Electronics Laboratory
Department of Electrical and Computer Engineering
Ben-Gurion University of the Negev
P.O. Box 653, Beer-Sheva 84105, ISRAEL.
Phone: +972-8-646-1561; Fax: +972-8-647-2949;
Email: sby@ee.bgu.ac.il
Website: www.ee.bgu.ac.il/~pel

Abstract - **When driving constant voltage loads that call for the stabilization of the output current, rather than output voltage, the use of topologies that have an output current sourcing behavior could be advantageous. This study proposes and analyses a one-stage, zero current switched, high voltage gain current sourcing converter to drive such a load. The topology is based on the parallel resonant converter, but includes blocking diodes at the input bridge to assist the soft switching operation. The results of the theoretical analysis were used to develop large and small signal behavior models.**

The behavior of the proposed converter was tested experimentally on a 1.3kW prototype, which was fed from a low voltage source in the range of 20V to 32V. The circuit was controlled by dsPIC30F2020 (Microchip, USA).

Good agreement was found between the theoretical predications and the experimental results.

I. Introduction

The use of topologies that have an output current sourcing behavior can be advantageous when driving loads that have a constant voltage or "voltage source"-like characteristic. These loads include high and low pressure discharge lamps, the power line (in grid connected inverters), batteries (in electronic chargers) and magnetrons and require the stabilization of the output current rather than the output voltage. For example, if a converter is loaded by magnetron, as considered in this study, its output voltage will be determined by the load (magnetron), while the output current needs to be regulated by the converter.

It has been shown that converters with triangular shaped inductor currents can be considered to have a current sourcing behavior when operating under ZVS [1-3]. However, ZVS has a number of drawbacks in high power, low input voltage (and hence very high primary current) applications. In such cases, the current fed back to the bus at the commutation instance will cause considerable ringing due to the parasitics, the increasing EMI emission and the power loss. Another drawback is the fact that these converters are turned off under extremely high currents, which again increases the EMI emission and power loss. Other approaches based on series resonant converters [4-9] also have a number of deficiencies in the application domain considered here. One major deficiency is the fact that they require a series resonant capacitor that needs to carry the large primary current. Consequently, these capacitors need to have extremely low ESR values which are just beyond the specifications of present day, commercially available capacitors. Furthermore, true soft switching in series resonant converters is normally achieved at the expense of high peak and rms currents [7].

Considering the above, this study explored the possibility of applying a parallel resonant converter that does not require a series capacitor, has a current sourcing output characteristic and runs under ZCS conditions.

II. Analysis of Proposed Topology

The traditional parallel resonant converter [10-13], with a parallel capacitor located at the secondary side of the isolating transformer and a voltage doubler at the output, is depicted in Fig. 1. Output power is controlled by varying the switching frequency. In the conventional operation of this converter, the turn-off of transistors occurs at non-zero current. In high input current applications, this non-zero current turn-off, poses a severe problem due to the switching losses and the injection of the high current back to the bus. This could be circumvented by operating at the matching switching frequency that will reduce the inductor current at turn-off to zero. However, this is possible only for one power point, while for other power levels non-zero current switching will still persist.

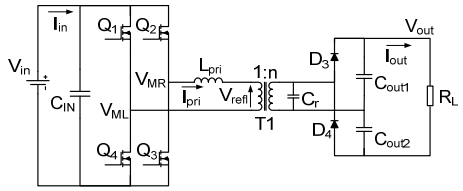

Fig. 1. Parallel resonant converter with output voltage doubler.

To preserve zero current switching at turn-off while still enabling output power control, it is proposed to introduce two series diodes as shown in Fig. 2 [14]. These would allow the inductor current to drop to zero while blocking the discharge current of the resonant capacitor, C_r. A detailed analysis of operational modes of this converter is given in [14]. For the sake of brevity, only the basic essentials will be repeated here.

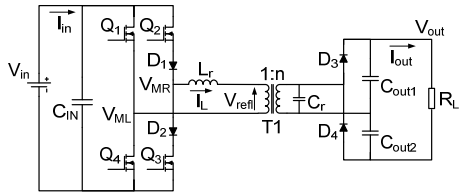

Fig. 2. Proposed topology with input diodes.

The key waveforms of this topology are sketched in Fig. 3. It is assumed that the forward voltage drop of the diodes D_1 and D_2 is much lower than the input voltage.

For this topology, four operational stages can be identified (Fig. 3):

a: time period t_0-t_1 (resonant phase).

Q2, Q4 and D1 are turned on under ZCS conditions (at t_0) and the voltage across capacitor C_r charges from $-V_{out}/2$ to $V_{out}/2$ by the sinusoidal-shaped inductor current due to the resonance of L_r and C_r. The inductor current and the capacitor voltage during this time interval are given as follows:

$$i_L^*(t) = (1+k)\sin(2\pi f_r t) \quad (1)$$

$$v_{Cr}^*(t) = n\left[1-(1+k)\cos(2\pi f_r t)\right] \quad (2)$$

where $i_L^*(t) = i_L(t)/(V_{in}/Z_R)$ and $v_{Cr}^*(t) = v_{Cr}(t)/V_{in}$ are the normalized inductor current and capacitor voltage, respectively, $k = V_{out}^*/2n$, $V_{out}^* = V_{out}/V_{in}$ is the normalized output voltage and $f_r = 1/(2\pi\sqrt{L_r C_r})$.

The t_0-t_1 time interval ends when the voltage across the capacitor reaches half of the output voltage (in the voltage doubler configuration). At this point in time, the relevant output diode starts to conduct (diode D_3 in Fig. 3), clamping the voltage across the capacitor C_r to $V_{out}/2$. The duration of this interval (t_1-t_0=t_1) and the normalized inductor current at its end, I_{t1}^*, are given as follows:

$$t_1 = \frac{1}{2\pi f_r}\arccos\left(\frac{1-k}{1+k}\right) \quad (3)$$

$$I_{t1}^* = (1+k)\sin\left(\arccos\frac{1-k}{1+k}\right) = 2\sqrt{k} \quad (4)$$

where $I_{t1}^* = I_{t1}/(V_{in}/Z_R)$ is the normalized inductor current at the end of the resonant phase and $Z_R = \sqrt{L_r/(n^2 C_r)}$ represents the characteristic impedance of the resonant network.

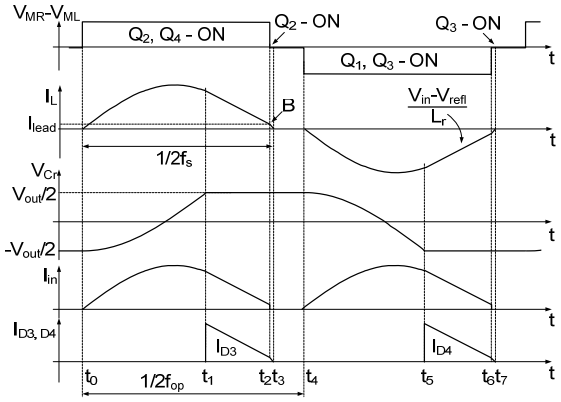

Fig. 3. Key waveforms of the proposed converter.

b. time interval t_1-t_2:

During this time interval, the voltage across the capacitor is clamped to $V_{out}/2$, output diode D_3 conducts and current is delivered to the load (I_{D3} in Fig. 3). Since the inductor is now clamped to constant voltages (V_{in} and $V_{out}/2n$), its current drops linearly. During this time interval, I_L can be expressed as follows:

$$i_L^*(t) = 2\sqrt{k} - \omega_r(k-1)(t-t_1), \text{ where } \omega_r = 1/\sqrt{L_r \cdot n^2 C_r} \quad (5)$$

After the inductor current drops to zero, transistor Q4 can be turned off at zero current. If some residual current, I_{lead}, is allowed (point "B", Fig. 3), it will maintain zero voltage switching at turn-on of transistor Q1.

The duration of this time interval is given by (6) (I_{lead} assumed to be negligibly small):

$$t_2 - t_1 = \frac{2}{\omega_r}\frac{\sqrt{k}}{k-1} \quad (6)$$

c. time interval t_2-t_3:

During this time interval the residual current of the inductor, if allowed, flows via D1 and Q2 and recharges the body capacitors of Q1 and Q4 (not shown in Fig. 3). Assuming that enough energy is stored in the inductor at the beginning of this time interval (depending on I_{lead}), the voltage across the transistor Q1 will drop to zero and its body diode will conduct, so that it can be turned on under zero current and zero voltage at the next switching half cycle.

d. time interval t_3-t_4:

Transistor Q2 is turned off under zero current. The inductor current is zero during this time interval. At nominal (maximum) power level this time interval will be negligibly short.

Based on the fact that the current is outputted to the load only during t_1-t_2 and assuming that I_{lead} is negligibly small, the normalized average load current was found to be:

$$I_{avout}^* = \frac{k}{\pi n(k-1)}\frac{f_{op}}{f_r} \quad (7)$$

where $I_{av\,out}^* = I_{av\,out}/(V_{in}/Z_R)$, $f_r = 1/2\pi\sqrt{L_r \cdot n^2 C_r}$ and f_{op} is operating frequency.

The output power delivered to the load is:

$$P_{out}^* = I_{av\,out}^* 2kn = \frac{2k^2}{\pi(k-1)}\frac{f_{op}}{f_r}, \quad P_{out}^* = \frac{P_{out}}{V_{in}^2/Z_r} \quad (8)$$

The incremental output impedance of the converter, R_o, was found by taking the derivative of $I_{av\,out}$ with respect to V_{out}:

$$R_o = \left(\frac{\partial I_{avout}}{\partial V_{out}}\right)^{-1} = \left(\frac{1}{2n\cdot Z_r}\frac{\partial I_{avout}^*}{\partial k}\right)^{-1} = -2\pi\cdot Z_r \cdot n^2(k-1)^2\frac{f_r}{f_{op}} \quad (9)$$

Fig. 4 shows the load characteristic of the magnetron considered in this study and the output characteristic of the proposed converter, which is plotted according to (7) and verified by cycle-by-cycle simulations (the simulations were performed on a power electronics simulator PSIM, version 7.1; Powersim, USA). It follows from the load characteristics of the magnetron that for a current range of 20mA to 350mA the voltage across it varies by only 13%. This implies that the magnetron can be modeled as a voltage source of about 3.9kV with a relatively small internal resistance of about 1.5kOhm. If the magnetron was driven by a converter with a small output resistance (which is typical of a voltage source), a small change in the magnetron's voltage would have caused a runaway of the output current so that a dedicated current control loop would have to be applied. On the other hand, if the magnetron is driven by the proposed converter a considerable change in the output voltage will only result in a minor change in the output current. This follows from inspection of the output characteristic of the proposed converter (line (2) on Fig. 4) - a voltage drop of about 400V (from a nominal value, 4.3kV, to a minimum operating voltage of the magnetron, 3.9kV), which covers almost the whole operational range of the magnetron, results in about 25mA variation in the output current (less than 10% of the nominal value). The low sensitivity of the output current in the proposed converter can be explained by its relatively high output impedance, as is normally expected in current sourcing applications. The corollary of this current sourcing behavior is that, theoretically, no current control feedback loop is necessary when driving a load with low internal resistance, like a magnetron.

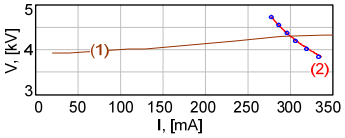

Fig. 4. Load characteristic of magnetron (1) and typical output characteristic of proposed resonant converter (2): solid line – calculated according to (7); dots – cycle-by-cycle simulation results.

IV. Behavioral Model of the Parallel Resonant Converter with Series Diodes

Since the average value of the inductor current is zero, the behavioral model will be developed with respect to the rectified inductor current. The basic form of this model is shown in Fig. 5

(the horizontal line above the symbols denotes the value, averaged over the switching cycle).

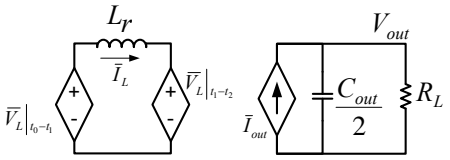

Fig. 5. Basic form of the behavioral model of proposed converter.

In this model, the inductor, L_r , is fed by two behavioral voltage sources. The magnitude of the left source is equal to the average voltage across the inductor during the resonance phase t_0–t_1 (Fig. 3), whereas the dependent source on the right of the inductor represents the average voltage across the inductor during the time interval t_1–t_2. The current to the output side of the converter (voltage doubler and the load) is set by the behavioral current source, $\bar{I}_{out}$. The output capacitor, $C_{out}/2$, represents the capacitance of the voltage doubler capacitors and R_L is the load.

During the time interval t_0–t_1 the voltage applied to the inductor is the difference between the input voltage and the resonant capacitor voltage reflected to the primary (V_{refl}, see Fig. 2). Thus, the net voltage across the inductor during this time interval is:

$$v_L(t)\Big|_{t_0-t_1} = V_{in} - \frac{v_{Cr}(t)}{n} \tag{10}$$

Considering (2), the average value of this voltage is:

$$\bar{V}_L\Big|_{t_0-t_1} = 2F_{op}\int_0^{t_1} v_L(t)\Big|_{t_0-t_1} dt = \frac{4F_{op}}{w_r}\sqrt{\frac{V_{in}V_{out}}{2n}} \tag{11}$$

where F_{op} is the switching frequency.

Eq. (11) determines the magnitude of the behavioral voltage source applied to the left side of the inductor in Fig. 5.

During the time interval t_1–t_2, the voltage across the resonant capacitor is clamped to $V_{out}/2$ and consequently the net voltage across the inductor is:

$$v_L(t)\Big|_{t_1-t_2} = \frac{V_{out}}{2n} - V_{in} \tag{12}$$

The average value of this voltage is:

$$\bar{V}_L\Big|_{t_1-t_2} = 2F_{op}\int_{t_1}^{t_2} v_L(t)\Big|_{t_1-t_2} dt = 2F_{op}\left(\frac{V_{out}}{2n} - V_{in}\right)(t_2 - t_1) \tag{13}$$

Since the current is delivered to the load only during the time interval t_1–t_2, the average value of the inductor current in this time interval must be equal to the average output current reflected to the primary side of the transformer, that is:

$$\bar{I}_L\Big|_{t_1-t_2} = \bar{I}_{out}\cdot 2n \tag{14}$$

where $\bar{I}_{out}$ is the average load current. The factor 2 is the current transfer ratio of the output voltage doubler.

The current in the inductor during t_1–t_2 is triangular and hence one can write:

$$\bar{I}_L\Big|_{t_1-t_2} = \frac{I_{L\,pk}\big|_{t_1-t_2}}{2} 2F_{op}(t_2 - t_1) = F_{op}\cdot(t_2 - t_1)\cdot I_{L\,pk}\Big|_{t_1-t_2} \tag{15}$$

Considering the fact that the voltage applied to the inductor during this time interval is $\frac{V_{out}}{2n} - V_{in}$, the peak current, $I_{L\,pk}\big|_{t_1-t_2}$, is:

$$I_{L\,pk}\Big|_{t_1-t_2} = \left(\frac{V_{out}}{2n} - V_{in}\right)\frac{t_2 - t_1}{L_r} \tag{16}$$

Substituting (16) into (15), equating to (14) and solving for t_2–t_1 yields:

$$t_2 - t_1 = 2n\sqrt{\frac{L_r\bar{I}_{out}}{V_{out} - 2nV_{in}}} \tag{17}$$

Applying (17) to (13) and rearranging yields the expression for the right voltage source of Fig. 5:

$$\bar{V}_L\Big|_{t_1-t_2} = 2\sqrt{L_r F_{op}\bar{I}_{out}(V_{out} - 2nV_{in})} \tag{18}$$

The magnitude of the output current source can be found by applying the relationship between the average inductor and output currents. During the time interval t_0–t_1 the inductor current recharges the resonant capacitor, whereas during t_1–t_2 it is delivered to the load. Consequently, the average inductor current can be represented as a sum of the average capacitor and output currents reflected to the primary side of the transformer:

$$\bar{I}_L = \bar{I}_{Cr}\cdot n + \bar{I}_{out}\cdot 2n \tag{19}$$

where $\bar{I}_{Cr}$ is the average current of the resonant capacitor.

Every half switching cycle the resonant capacitor is recharged from ($V_{out}/2$) to ($-V_{out}/2$), so the charge transferred to it is $Q_{Cr} = V_{out}C_r$. Consequently, the average capacitor current is

$$\bar{I}_{Cr} = 2F_{op}Q_{Cr} = 2F_{op}V_{out}C_r \tag{20}$$

Substituting this into (19) yields an expression for the dependent current source of Fig. 5:

$$\bar{I}_{out} = \frac{\bar{I}_L}{2n} - C_r F_{op} V_{out} \tag{21}$$

Fig. 6 presents the behavioral average model of the converter after applying (11), (18) and (21) for the dependent sources.

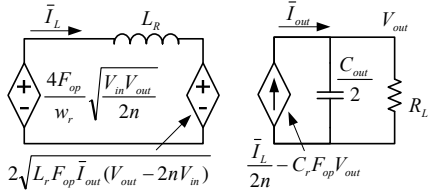

Fig. 6. Behavioral model of converter.

The behavioral model of Fig. 6 was further used to obtain the small signal responses of the proposed converter. Since the bandwidth of control loops in practical applications is bounded by a few kilohertz, small signal excitation frequencies above a few kilohertz are beyond the scope of interest for small signal analysis. On the other hand, the main inductor, L_r , will be typically driven by relatively high switching frequencies of, say, several dozens of kilohertz or even higher. The inductor impedance, which is proportional to this switching frequency, will be fairly high as well. Therefore, a (relatively) slow small signal disturbance or excitation will have very little effect on the inductor impedance. Putting this in other words, the change in inductor impedance due to a small signal excitation (the impedance variation) will be negligibly small as compared to its quiescent value. Consequently, while deriving the small signal model of the converter, the inductor of Fig. 6 can be shorted, reducing the average model to a first order model.

a) Small signal output voltage response to a modulating frequency, derived by applying the first order average model.

In practical applications it is usually desirable to maintain constant voltage at the output. One possible way to achieve this in the proposed converter is to control the switching frequency. That is, the control transfer function required for the design of the

compensation network is the response of the output voltage to a modulation of f_{op} in the switching frequency. To find the dependence of the output voltage changes, v_{out} , on a small signal variation of the switching frequency, f_{op}, the behavioral model was first linearized by taking a derivative of the dependent sources of Fig. 6 with respect to f_{op}. The resulting small signal model (the inductor is shorted) is presented in Fig. 7.

The relationship between i_{out} and v_{out} was found from the output side subcircuit of Fig. 7:

$$i_{out} = \frac{v_{out}}{R_L}\left(1 + s\frac{C_{out}}{2}\right) \qquad (22)$$

By equating v_1 and v_2 (Fig. 7) and applying (22), the output voltage to switching frequency transfer function is found to be:

$$\frac{v_{out}}{f_{op}} = \frac{I_{out}}{F_{op}} R_{eq} \frac{1}{1 + j\dfrac{f}{1/2\pi C_{eq} R_{eq}}} \qquad (23)$$

where $R_{eq} = R_L(1 - 2n/Gain)$, $C_{eq} = C_{out}/2$ is the equivalent output capacitance and $Gain = V_{out}/V_{in}$ is the voltage gain of the converter.

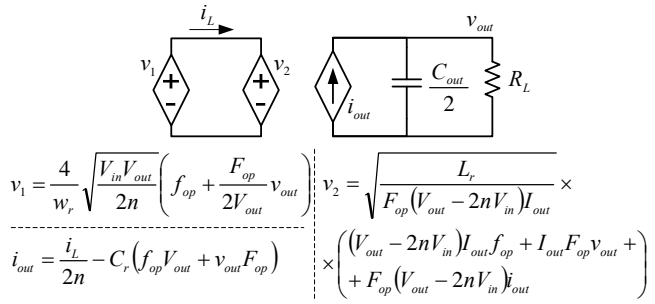

Fig. 7. Linearized average small signal model of the converter for small signal excitation in F_{op}, (f_{op}).

Eq. (23) implies that the output voltage response to the switching frequency small signal variations is of the first order, so it can be easily compensated for by a simple compensation network. It also follows that for some specific design, the product of the pole frequency of (23) and its "zero" frequency magnitude is constant and equals $\frac{I_{out}}{C_{eq}}\frac{1}{2\pi F_{op}}$. The transfer function of (23) has a low frequency gain of $\frac{I_{out}}{F_{op}}R_{eq}$ and a pole at $\frac{1}{2\pi C_{eq}R_{eq}}$ and hence the small signal model of Fig. 7 can be further reduced to the following equivalent circuitry:

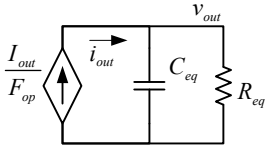

Fig. 8. Circuit representation of (23)

b) Small signal output current response to a modulating frequency

In applications with a load having "voltage source" like characteristics (e. g. magnetron), the control transfer function required for the design of the compensation network would be the response of the output current to a modulation of f_{op} in the switching frequency. To find this transfer function, the dependent sources of Fig. 6 were linearized again, assuming that the disturbance is in the switching frequency. Both, the input and the output voltages were assumed to be constant. The small signal output current to frequency transfer function was found to be:

$$\frac{i_{out}}{f_{op}} = \frac{I_{out}}{F_{op}} \qquad (24)$$

c) Behavioral model verification

The behavioral model of Fig. 6 was verified by cycle-by-cycle simulations (PSIM, version 7.1; Powersim, USA).

The frequency response of the output voltage to the frequency excitation was obtained by running the cycle-by-cycle simulation model in the time domain for different excitation frequencies. For every excitation frequency, the output voltage signal at the same frequency was measured and compared to that of the excitation source. The results, shown in Fig. 9, were plotted for an input voltage of 24V, switching frequency of 50kHz and a transformer ratio of 48. Fig. 9 shows the excellent agreement between the output voltage–to–switching frequency responses obtained from the cycle-by-cycle simulation model (solid lines in Fig. 9) and from the behavioral model of Fig. 6 (dashed lines). The disagreement in phase observed at high frequencies can be explained by the error found in the cycle-by-cycle simulation when the excitation frequency approaches half the switching frequency.

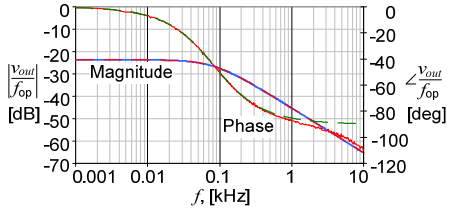

Fig. 9. Output voltage–to–switching frequency transfer function.
Solid lines: cycle-by-cycle simulation results.
Dashed lines: calculated from the behavioral model of Fig. 7.

The same simulation model was used to obtain the output-current to switching-frequency transfer function. The simulation results were compared to those obtained from the behavioral model (Fig. 10).

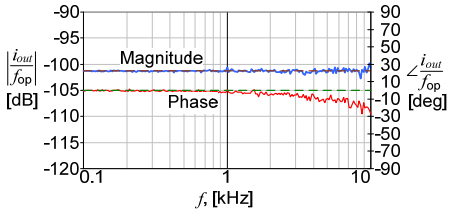

Fig. 10. Output-voltage to switching- frequency transfer function.
Solid lines: cycle-by-cycle simulation results.
Dashed lines: calculated from the behavioral model.

VII. Experimental Study

The behavior of the proposed converter was tested experimentally on a 1.3 kW prototype that was built according to the topology shown in Fig. 2. The transformer ratio, n, was set to 48. The primary winding of the transformer had four turns. The leakage of the transformer T1, used as a main inductor, L_r, was about 0.8 µH. The resonant capacitor, C_r , was chosen to be 2.2 nF and the output capacitors, C_{out1} and C_{out2} , were 0.5 µF each. The input voltage range was from 22 V up to 32 V and the switching frequency varied from about 30 kHz at the maximum input voltage up to about 55 kHz when the input voltage was lowest. The input

bridge consisted of IRFP4368 (International Rectifiers, USA) MOSFETs with typical Rdson of 1.46 mΩ@25^{0}C. The input diodes, D1 and D2, were DSS 2x160-01A (IXYS, USA) each (2 Schottky diodes that were connected in parallel). The output diodes, D3 and D4, were HVUFS7500 (HV Components/CKE, USA). The circuit was governed by a dsPIC30F2020 (Microchip, USA). The experiments were carried out for two different load types (resistor and magnetron) with and without output current regulation. When the regulation was applied, the output current was controlled by varying the switching frequency. The experimental circuit was fed from a low input voltage source in the range of 20V to 32V, while maintaining a high voltage (about 4.3kV) at the output. The output current was set to about 300mA.

Fig. 11 shows typical experimental results with a magnetron at nominal output power. The input voltage was 23V and the output voltage was about 4.3kV. In this experiment, the magnetron was attached to a waveguide that was terminated by a dummy load. The microwave power was measured by means of a diode detector 423B (Agilent, USA). The electrical efficiency at nominal output power (1.3kW), measured at different operating points, varied from 85% at a low input voltage (22V) up to 88% at Vin=28V.

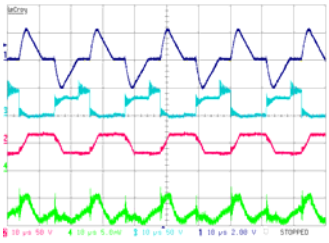

Fig. 11. Typical experimental results; loaded by magnetron. Upper trace: Inductor current 200A/div; Second trace from top: V_{MR} (Fig. 2) 50V/div; Third trace from top: Transformer primary voltage 100V/div; Lower trace: Microwave power 880W/div; Horizontal scale: 10us/div.

V. Discussion and Conclusions

This paper describes a one stage, high voltage gain, current sourcing converter topology that was implemented within the design of a battery operated (24V) 1.3kW magnetron driver. The converter does not require a series capacitor which makes it possible to operate at high input currents (100Arms and above).

The analytical results of this study were used to develop large and small signal behavioral models and were verified by simulations and experimental results. All are in good agreement with the theoretical predictions.

The major advantages of the proposed topology and mode of operation are soft switching and output current sourcing. All the switches and input diodes are operated at ZCS at turn-on and turn-off, while the output diodes (high voltage low current) are turned on under ZVS and turned off under ZCS. The ZCS operation at the primary and the smooth, sinusoidal-like current are extremely beneficial in high primary current cases since they reduce the ringing due to the parasitic inductances of the power elements and the wiring. The inherent current sourcing at the output of the proposed converter eases the current control task by reducing the sensitivity of the output current to source and load voltage variations. This reduced sensitivity of the output current can be explained by the relatively high output incremental resistance (eq. (9)). For example, in the proposed converter the open loop incremental output resistance is in the range of several kilo ohms. In the conventional (e.g. PWM) converter the open loop output resistance will be determined by the parasitic resistances of the inductor and the wirings and, consequently, will be in the order of several ohms or even less. This high output resistance attribute is especially important in the present magnetron driver application, considering the low incremental resistance of the magnetron. The high output impedance is a direct consequence of the fact that the proposed converter exhibits a current sourcing behavior at the output.

References

[1] I. D. Jitaru, “A 3 kW soft switching DC-DC converter,” IEEE Fifteenth Annual Applied Power Electronics Conference and Exposition, APEC 2000, vol. 1, pp. 86 – 92, 6-10 Feb. 2000.

[2] F. Krismer, J. Biela, and J. W. Kolar, "A Comparative Evaluation of Isolated Bi-directional DC/DC Converters with Wide Input and Output Voltage Range," *IEEE Industry Applications Conference, Fourteenth IAS Annual Meeting, vol. 1, pp. 599 - 606, 2-6 October 2005*.

[3] I. Zeltser and S. Ben-Yaakov, "Transformer's capacitance effect on the operation of triangular-current shaped soft-switched converters," *IEEE Applied Power Electronics Conference, APEC-2010, 928-934, Palm Springs, CA, 2010.*

[4] R. L. Steigerwald, " Analysis of a resonant transistor DC-DC converter with capacitive output filter", *IEEE Transactions on Industrial Electronics, vol. IE-32, no. 4, November 1985, pp. 439-444*.

[5] A. K. S. Bhat, " Analysis and design of a series-parallel resonant converter with capacitive output filter", *IEEE Transactions on Industry Applications, vol. 27, no.3, May/June 1991, pp. 523-530.*

[6] J. Liu, L. Sheng, J. Shi, Z. Zhang, X. He, "LCC Resonant Converter Operating under Discontinuous Resonant Current Mode in High Voltage, High Power and High Frequency Applications," *IEEE Applied Power Electronics Conference, APEC-2009, 1482-1486, Washington, DC, 2009.*

[7] B.M. Hasanien, K. F.A. Sayed, "Current Source ZCS PFM DC-DC Converter for Magnetron Power Supply," *International Middle-East Power System Conference, MEPCON 2008, 464-469, Aswan, Egypt, 2008.*

[8] H. Takano , T. Hatakeyama, L. Gamage, J.M. Sun, and M.Nakaoka, "Novel Digital Control Topology of a high Power Resonant DC-DC Convertert for X-Ray High Voltage Applications," *Proceedings of the Power Conversion Conference – Nagaoka 1997, vol. 2, 1031-1018, Nagaoka, Japan, 1997.*

[9] F. da S. Cavalcante and J. W. Kolar, " Small-Signal Model of a 5kW High-Output Voltage Capacitive-Loaded Series-Parallel Resonant DC-DC Converter," *IEEE Power Electronics Specialists Conference, PESC 2005, 1271-1277, Recife, Brazil, 2005.*

[10] S. D. Johnson and R. W. Erickson, "Steady-state analysis and design of the parallel resonant converter", *IEEE Transactions on Power Electronics. vol. 3, no.1, 1988, pp. 93-104.*

[11] G. Ivensky, A. Kats, and S. Ben-Yaakov, "An RC load model of parallel and series-parallel resonant DC-DC converters with capacitive output filter," *IEEE Trans. on Power Electronics, 14, 3, 515-521, 1999.*

[12] A. Bucher, T. Duerbaum, and D. Kuebrich, "Comparison of Methods for the Analysis of the Parallel Resonant Converter with Capacitive Output Filter," *European Conference on Power Electronics and Applications, 2007, 1-10, Aalborg, Denmark, 2007.*

[13] M.P. Theodoridis, "Analysis of a capacitive-filter, half-wave rectifier fed by a parallel-load resonant tank," *IEE proceedings – Electric Power Applications, vol. 152, 878-884, 2005.*

[14] I. Zeltser and S. Ben Yaakov, "Current sourcing ZCS magnetron driver for low input voltage applications," *IEEE Applied Power Electronics Conference, APEC-2011, 877-884, Fort Worth, TX, 2011.*